PAPER

CrossMark
← click for updates

Plasma modification of poly(2-heptadecyl-4-vinylthieno[3,4-d]thiazole) low bandgap polymer and its application in solar cells†

Pankaj Attri,[a] Vishal Bharti,[b] Young Sun Kim,[c] Jitender Gaur,*[b] Suresh Chand,[b] Gi-Chung Kwon,[a] Seung-Hyun Lee,[d] Weontae Lee,[e] Eun Ha Choi*[a] and In Tae Kim*[c]

For the first time, we here propose a green methodology to modify a low bandgap polymer for highly efficient solar cells using atmospheric pressure plasma jet or soft plasma operating on different feeding gases (air, Ar and N_2). The physical properties of the modified polymer were investigated using conductivity measurements, UV-visible spectroscopy, photoluminescence spectroscopy, X-ray photoelectron spectroscopy, cyclic voltammograms, atomic force microscopy, cathodoluminescence and confocal Raman spectroscopy. Further, we examined the variation of the work function of the polymer before and after plasma treatment using a γ-focused ion beam. Additionally, photovoltaic cells based on the plasma-modified polymer having ITO/PEDOT:PSS/PHVTT (with or without plasma modification):$PC_{71}BM$/LiF/Al configuration were fabricated and then characterized. We found that the power conversion efficiency (PCE) of the plasma-modified polymer increased dramatically as compared to the control polymer (without plasma treatment). PCE of the control polymer was found to be 4.11%, while after air, Ar and N_2 gas plasma treatment the polymer showed PCEs of 4.85%, 4.87% and 5.14% respectively. Thus, plasma treatment not only alters the surface properties, but also modifies the bulk properties (changes in HOMO and LUMO bandgap level). Hence, this work provides new dimensions to explore more about plasma and polymer chemistry.

1. Introduction

The scientific and technological communities have made numerous efforts to create, sustain and apply plasmas due to their several applications in various areas. These associate a number of fields, such as physics, chemistry, biology, engineering, medicine and microbiology, into multidisciplinary research. Due to significant industrial advantages, the atmospheric pressure non-thermal plasma jet (APPJ) has attracted more attention than low-pressure discharge. APPJ has some attractive features for generating unique chemistry.[1–3] It can produce a stable, uniform and homogenous discharge at atmospheric pressure. APPJ can function without a dielectric cover over the electrode, and hence it is free from filaments, arcing and streamers, and can work at low discharge gas temperature, permitting it to treat delicate surfaces without damage.[1,4–9]

Polymer surface modification is a useful method for creating functional polymer surfaces combined with the necessary features of bulk polymers.[10–15] There are several advantages of the use of plasmas for the treatment of solid surfaces over the conventional solution phase chemistry. Plasma processes are energy efficient and solvent free, rendering them a cost-effective and environmentally friendly alternative to traditional methods.[10–12] There are many polymers that have been modified using different types of plasma sources.[10–15] Modification has not been done on low bandgap polymers, nor has their utility in bulk heterojunction solar cells been studied so far. Low bandgap polymers have attracted much attention due to the wide range of small and large applications in organic photovoltaic devices (OPVs).[16–25] With an aim of enhancing the efficiency of polymer solar cells (PSCs), we developed a polymer, namely poly(2-heptadecyl-4-vinylthieno[3,4-d]thiazole) (PHVTT),[26] and modified it with APPJ in the presence of different feeding gases (air, Ar and N_2) and further examined its utility for increasing the efficiency of PSCs.

[a] *Plasma BioScience Research Center/Department of Electrophysics, Kwangwoon University, Seoul, Korea 139-701. E-mail: ehchoi@kw.ac.kr; Fax: +82-2-909-1978; Tel: +82-2-3795-1479*

[b] *Council of Scientific and Industrial Research-National Physical Laboratory, Dr. K. S. Krishnan Marg, New Delhi-110012, India. E-mail: jitender.jnsri@gmail.com*

[c] *Department of Chemistry, Kwangwoon University, Seoul, Korea 139-701. E-mail: itkim@kw.ac.kr*

[d] *Graduate School of Information Contents, Kwangwoon University, Seoul, Korea 139-701*

[e] *Department of Biochemistry, College of Life Science & Biotechnology, Yonsei University, Seoul, 120-749, Korea*

† Electronic supplementary information (ESI) available. See DOI: 10.1039/c4cp03323j

This journal is © the Owner Societies 2014

Phys. Chem. Chem. Phys., 2014, **16**, 27043–27052 | **27043**

This provides details of the mechanism and scope for newer applications in the field of solar cells.

2. Experimental section

2.1 Materials

The reagents used for the synthesis of the polymer were supplied by Aldrich Chemical Co. (USA). All chemicals and reagents were used without any further purification. The synthesis and characterization of PHVTT[26] are described in the ESI.†

2.2 Characterization methods

The synthesized compounds were identified by ^{1}H NMR and ^{13}C NMR spectra, recorded with a Jeol MSL 300 spectrometer. Gel permeation chromatography was carried out with polystyrene standards prepared in THF solutions. A UV-visible S-3100 spectrophotometer having wavelength resolution of 0.95 nm, wavelength accuracy of ± 0.5 nm and wavelength reproducibility of ± 0.02 nm was utilized for the analysis. Raman spectra were measured at room temperature using a confocal Raman microscope (WITec, Alpha 300 R) with a 632.8 nm He–Ne laser. Electrical conductivity measurements were performed using standard four-in-line probe apparatus. The thickness of polymer thin films was measured by an Alpha-Step profilometer. An XE-100 atomic force microscopy (AFM) Park system, Korea, was used for the characterization. High-resolution X-ray photoelectron spectroscopy (XPS) experiments were performed on the PLS-8A1 undulator (U7) beam line equipped with a variable-included-angle plane-grating monochromator, Japan. Cyclic voltammograms (CV) were from CH Instruments, USA. Cathodoluminescence (CL) experiments were carried out using a MonoCL3 purchased from Gaton (UK). The film thicknesses of PHVTT films used for the electrical conductivity, AFM, XPS, Raman spectra and CL measurements were 39 μm.

2.3 APPJ device

The key components of the soft plasma jet system are electrodes, dielectrics, and a high-voltage power supply.[6,7] The AC power supply is a commercially available neon light transformer operating at 60 Hz and is connected to two electrodes. The primary voltage of the high-voltage transformer is regulated with the help of a voltage controller. The inner electrode is a typical injection needle made of stainless steel having an inner diameter of 1.2 mm with a thickness of 0.2 mm; it is tightly covered with a quartz tube having an outer diameter of 3.2 mm. The quartz tube is inserted through the inner electrode which is machined using porous alumina 10 mm in diameter and 20 mm in length. The tip of the inner electrode is placed in contact with the inner surface of the porous alumina. The outer electrode with a conical shape is fabricated from stainless steel, and the plasma jet is ejected to the surrounding ambient air through a centrally perforated hole of 1 mm. The porous alumina with the inner electrode is installed within the outer electrode. The distance between the tips of the porous alumina and the inner electrode is referred to as the discharge gap (dg; in this work, dg is 2 mm)

which could be adjusted by controlling the depth at which the inner electrode was inserted into the porous alumina. The inner surface of the outer electrode is also in contact with the tip of the porous alumina. Air is injected into the injection needle through a 1 mm hole in the outer electrode *via* the porous alumina. The alumina used for the inner electrode had approximately 30% vol. porosity with an average pore diameter of 100 μm. Once air is introduced through the inner electrode and high-voltage AC power is applied, a discharge is fired in the porous alumina between the electrodes, generating a long plasma jet reaching up to several centimeters in length which is ejected into the open air. Compressed atmospheric dry air, Ar and N_2 gas with a purity of 99.9999% were used at a flow rate of 1 liter min^{-1}, which can be adjusted and measured by a mass flow controller.

We can determine the plasma parameters of electron temperature using a high-speed image-intensifying camera which can record the temporal propagation distance *versus* elapsed time. Recording the average value of temporal distance Δx *versus* time interval Δt can help in obtaining the average plasma propagation speed for the ionization front as $v = \dfrac{\Delta x}{\Delta t} = 0.7$ cm μs^{-1}. This plasma speed can then be expressed by the relation $v = \sqrt{\dfrac{kT_e}{M}}$. Here the electron temperature kT_e can be experimentally measured as ~ 1.7 eV under different gases. Also the plasma density can be calculated from $n_e = \dfrac{I(t)}{2\pi e v \sigma^2} \exp\left(\dfrac{-r^2}{2\sigma^2}\right)$ where I is measured electric current, e is the electron charge, $v = \sqrt{\dfrac{kT_e}{M}} \sim 0.7$ cm μs^{-1} is the plasma propagation velocity determined by high speed image camera, and σ is a radial profile of the plasma jet determined by experiment. The electron temperature is ≈ 0.8–1.0 eV and plasma density is 2.0×10^{13} cm^{-3} in this experiment, using the atmospheric pressure collisional radiative model and ion collector current. The emission spectrum of N_2 gas plasma is shown in Fig. 1, whereas the air and Ar gas plasma emission spectra are illustrated in Fig. S1 and S2 (ESI†).
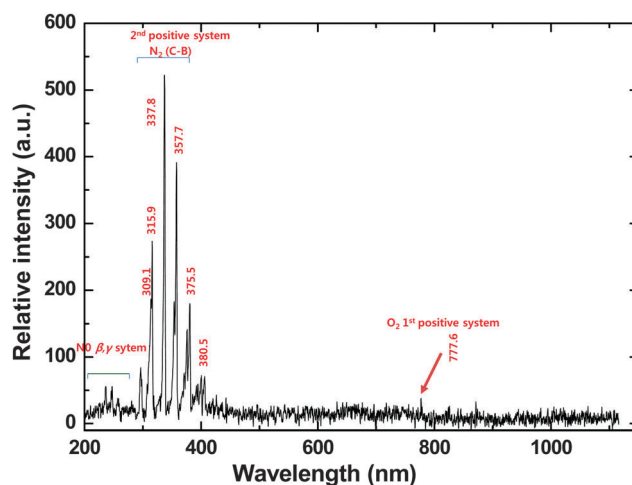
Fig. 1 The emission spectrum of atmospheric-pressure plasma jet (APPJ) with N_2 as feeding gas.

27044 | *Phys. Chem. Chem. Phys.*, 2014, **16**, 27043–27052

This journal is © the Owner Societies 2014

It was observed in this experiment that the VUV lines in the range 120–200 nm were easily absorbed by the atmospheric oxygen molecules. However, the emission lines beyond 200 nm easily passed through the oxygen molecules in the atmospheric air, which enabled us to explore the emission spectrum in the wavelength range of 200–1000 nm. Emission lines were observed for the molecular NO β, γ system between 200 and 250 nm and superoxide anion O_2^* at 245 nm as well as the emission line of 309.1 nm appearing for OH radicals in the case of all the feeding gas plasmas. We noticed that the emission spectra for the molecular N_2(C–B) second positive system for all air, N_2 and Ar feeding gas plasmas were concentrated in the wavelength range of 300–400 nm, whereas the emission spectra for molecular N_2^+(B–X) were seen as spectrum lines in the wavelength range of 450–600 nm, and those for N_2(B–A) were observed in the wavelength range of 600–700 nm, in the case of the air gas plasma only. Also, the emission lines for the O_2 first negative system were observed in the wavelength range of 470–620 nm, whereas typical 500.6 nm was a characteristic line in the case of the air gas plasma experiment. Also, the lines of the N_2 molecular first positive system appeared in the range of 700–900 nm in the case of the air plasma only. It is necessary to mention that the oxygen atom O lines appearing at 777.6 nm were observed in the cases of all feeding gas plasmas, while the peak at 844.8 nm for O lines was evident only in the case of air and Ar gas feeding plasmas.

2.4 Work function and secondary electron emission coefficient of polymer and modified polymer using γ-focused ion beam (γ-FIB) system

In order to examine the changes in the secondary electron emission coefficient ($γ$) and molecular energy band structure of the polymer due to atmospheric nonthermal plasma treatment, we used a γ-focused ion beam (γ-FIB) system in this experiment.[8,27] Fig. S3 (ESI†) shows a schematic view of the γ-FIB consisting of the ionization region of ions, thermal electron source, electrostatic single Einzel lens that focuses on the ion beam, and collector and copper pad for secondary electron emission measurements from the surface of the polymer thin films. We used He^+ ions whose ionization energy E_i is 24.58 eV, with low energy below 200 eV. The He^+ ions approach the surface of the polymer film. The electric field is polarized toward the collector from the grounded copper pad when the collector potential is negatively biased. The secondary electrons emitted from the surface by these slow ions then come back, and only the ion current (I_i) coming to the surface is then measured. On the other hand, a positively biased collector makes the electric field toward the grounded copper pad. Due to this electric field, the secondary electrons emitted from the surface of the thin polymer film by the ion beam bombardment move up towards the collector, registering a current (I_t) in the ampere meter, in which the emitted secondary electron and ion beam currents (I_i) are included together. The secondary electron emission $γ$ is obtained from $γ = (I_t - I_i)/I_i$.

2.5 Fabrication of polymer solar cell devices

The PSCs were fabricated based on the configuration ITO/ PEDOT:PSS/PHVTT:PC$_{71}$BM/Al *via* the following procedure.

ITO-coated glass substrates were thoroughly cleaned with a detergent, followed by treatment in an ultrasonic bath using different solvents in sequence: acetone, trichloroethylene and isopropanol. The cleaned substrates were then annealed at 150 °C in a vacuum oven for 20 min and subsequently exposed to UV ozone cleaning for 10–15 min. PEDOT:PSS (Sigma-Aldrich, USA, 1.3% dispersion in water) was spin-coated over the dried substrates using a digital spin coater with optimized spin for ~ 40 nm film thickness. After this, the substrates were dried at 140 °C for 30 min in a vacuum oven and then transferred into a glove box for deposition of the active layer on the substrate using the spin-cast technique. Polymer and PC$_{71}$BM (PC$_{71}$BM from Sigma-Aldrich, USA) were separately dissolved in chlorobenzene (20 mg ml^{-1}), followed by mixing of the two solutions. This mixture of PHVTT and PC$_{71}$BM was used to develop active layers of the device in a ratio of 1 : 1.5. The film thicknesses of PHVTT:PC$_{71}$BM in various devices were between 130 and 150 nm as measured by a stylus profilometer (Ambios XP200 Profiler). The active layer was spin-cast on the PEDOT:PSS film and cured at 140 °C for 20 min under nitrogen atmosphere in a glove box. Finally, aluminium electrodes of thickness of 120 nm were deposited through a shadow mask inside the thermal evaporator chamber having vacuum $\sim 8 \times 10^{-6}$ mbar. The active area of the pixel device prepared was ~ 0.075 cm^2. The current density–voltage (J–V) characteristics of the devices were recorded using a Keithley 2420 Source Meter unit interfaced with a computer, performed under a tungsten halogen lamp with illumination intensity of 1000 W m^{-2} with 1.5 air mass (AM 1.5G). The device performance was measured by the efficiency ($η$) and fill factor (FF). For each type of device, 5 specimens were fabricated with 4 pixels each and results are presented as the average of all 20 pixels. The efficiency of the solar cell is calculated as $η = \dfrac{V_{max} \times J_{max}}{1000}$. Here V_{max} and J_{max} are, respectively, the maximum voltage and maximum current drawn from the device. The FF is measured by $FF = \dfrac{η}{V_{oc} \times J_{sc}}$. Here V_{oc} is the open circuit voltage and J_{sc} is the short circuit current. However, variation in the device performance may be due to variation in the film thickness of hole transport layers and active layers as the spin-coating process of the respective materials can only produce film thicknesses in a range of values.[28]

3. Results and discussion

Recent development of low bandgap polymers allows the energy-level engineering of polymers for enhancing photovoltaic performance.[29–31] Hence, we synthesized and characterized the low bandgap PHVTT polymer as per our previously reported work.[26] The UV-visible absorption spectra of PHVTT (Fig. 2a) show the absorption onset of PHVTT polymer at 750 nm, indicating an optical bandgap. Therefore, we studied the bulk heterojunction photovoltaic cells, fabricated on the basis of ITO/PEDOT:PSS/ PHVTT:PC$_{71}$BM/LiF/Al configuration, and measured their performances under 100 mW cm^{-2}. PC$_{71}$BM was preferred over PC$_{61}$BM due to its stronger light absorption in the visible region.[23]
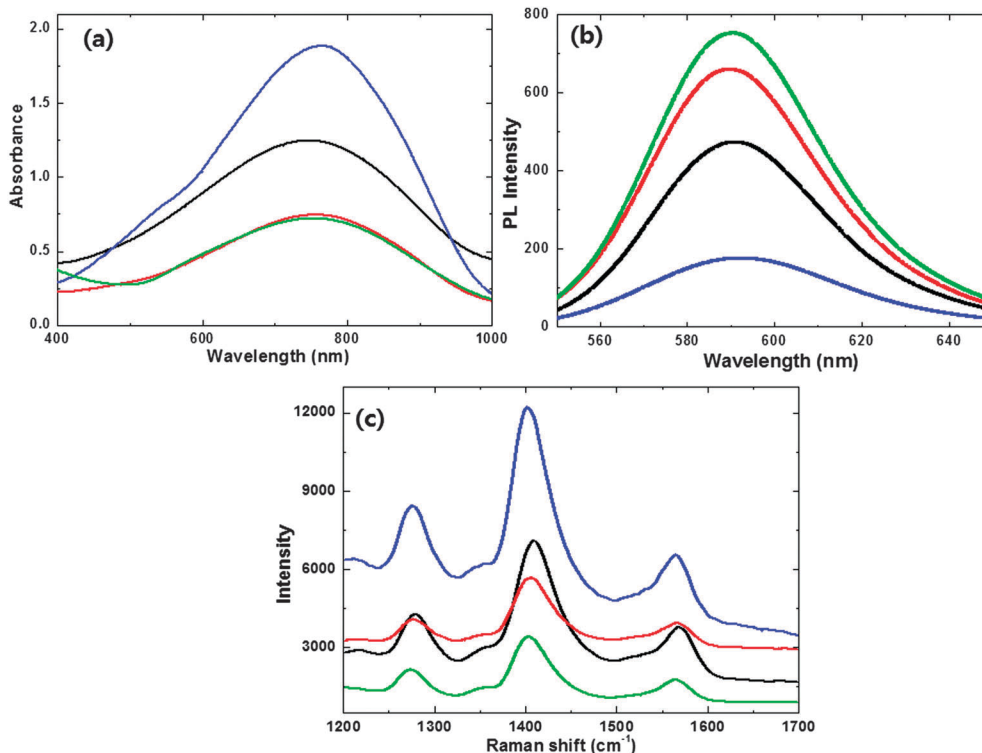
Fig. 2 (a) UV-visible absorption spectra, (b) photoluminescence (PL) spectra and (c) confocal Raman spectra of polymer (black), polymer treated with air plasma (red), polymer treated with N_2 plasma (blue) and polymer treated with Ar plasma (green).

Table 1 Photovoltaic and electrochemical properties of the PHVTT(1):PC$_{71}$BM(1.5) devices

Device	HOMO (eV)	LUMO (eV)	E_g (eV)	V_{oc} (V)	J_{sc} (mA cm^{-2})	FF (%)	R_{SH} ($\times 10^3$ Ω)	R_{SR} (Ω)	PCE (%)
PHVTT	−4.76	−3.63	1.13	0.72	10.43	54.09	105	748	4.11 (±0.03)
Air plasma	−4.77	−3.57	1.20	0.75	10.93	58.45	165	846	4.87 (±0.05)
N_2 plasma	−4.86	−3.62	1.24	0.79	11.00	58.13	213	818	5.14 (±0.03)
Ar plasma	−4.78	−3.57	1.21	0.75	10.93	58.31	160	846	4.83 (±0.04)

The devices based on PHVTT exhibit an efficiency of OPVs of 4.11%, as shown in Table 1. This is still less than the reported efficiency of many OPVs[29–31] and hence the synthesis of another new polymer using trial-and-error methods is not a good idea from the aspect of green chemistry. Therefore, we have used an APPJ operating with different feeding gases (air, N_2 and Ar) to modify the synthesized low bandgap polymer in order to enhance the efficiency of OPVs.

3.1 Characterization of modified polymer using UV-visible spectroscopy

The energy of particles and the depth of impact created by APPJ are the important parameters for polymer surface modifications. The chemical bonds on the polymer surface can be disrupted after the impact of an energetic particle resulting in a more reactive surface. Thus, new reactive functional groups can be created and the polymer surface can be modified up to a depth of a few hundreds or thousands of angstroms.[32] UV-visible spectroscopy provides substantial experimental results of the molecular modification of the polymer. After the treatment of the polymer with APPJ operating with different gases, the polymer spectrum exhibited a significant shift as compared to that of the control polymer (as displayed in Fig. 2a). The polymer showed a maximum absorption at 750 nm, while PHVTT + air plasma showed a maximum absorption at 764 nm with an intensity reduction. This shows that the air plasma strongly modifies the low bandgap polymer. On the other hand, in the case of the polymer + Ar plasma a red shift with maximum absorption at 765 nm was observed, with an intensity reduction slightly more than in the case of PHVTT + air plasma. The combination of N_2 plasma with the polymer also exhibited a red shift with a more intense maximum absorption at 767 nm. Thus, UV-visible spectroscopy results reveal that all the feeding gases of APPJ favorably modify the polymer surface.

3.2 Characterization of polymer and modified polymer using photoluminescence (PL) spectroscopy, confocal Raman spectroscopy and CV measurements

In order to gain more insight into the optical properties of the control polymer and plasma-modified polymer (polymer + plasma), we utilized PL spectroscopy, and the results are displayed in Fig. 2b. Maximum PL for the control polymer (without plasma treatment)

27046 | *Phys. Chem. Chem. Phys.*, 2014, **16**, 27043–27052

This journal is © the Owner Societies 2014

was observed at ≈590 nm, while the PHVTT + air plasma showed maximum PL at 589 nm with an enhanced intensity. This shows that, after air plasma treatment, the polymer showed a slightly blue wavelength shift, with increased intensity. On the other hand, there is no wavelength shift for polymer + Ar plasma as compared to polymer + air plasma, although the intensity of the peak increased more in the case of the Ar plasma-treated polymer. However, the N_2 plasma-treated polymer exhibited a red shift of 3 nm with intensity reduction as compared to the control polymer. Thus, PL spectroscopy results reveal that N_2 plasma treatment modified the PL spectra of the polymer to a greater extent as compared to plasma operating with the other feeding gases. To further investigate the modification of the low bandgap polymer, we made use of the confocal Raman spectroscopy.

In order to elucidate the modification of the polymer, we employed another reliable technique, confocal Raman spectroscopy, that allowed us to take advantage of the spatial resolution of the confocal microscope.[33,34] From Fig. 2c, we found that the polymer showed significant peaks at 1278, 1410 and 1568 cm^{-1}, while for the plasma-treated polymer we observed a blue shift that confirmed the modification of the polymer using APPJ. In the case of polymer + air plasma, we found broad Raman peaks at 1274, 1405 and 1566 cm^{-1} as compared to the control polymer, although wavelength shifts and quenched intensity were also observed in the spectrum of the air plasma-treated polymer at 1273, 1401 and 1564 cm^{-1}. On the other hand, sharp and highly intense peaks were detected for the N_2 plasma-treated polymer at 1274, 1400 and 1565 cm^{-1}. Hence, variation in wavelength shift, broadening and intensity of peaks in Raman spectra after plasma treatment revealed modification of the polymer to different extents using plasma operating with different feeding gases.

Additionally, CV was employed to examine the electrochemical properties and evaluate the HOMO and LUMO levels of the polymers. The results are shown in Table 1 and Fig. S4 (ESI†). The onset oxidation potentials $(E_{ox})_{on}$ for the polymer, polymer + air plasma, polymer + N_2 plasma and polymer + Ar plasma are 0.363 eV, 0.379 eV, 0.478 eV and 0.383 eV, whereas the onset reduction potentials $(E_{red})_{on}$ for the polymer, polymer + air plasma, polymer + N_2 plasma and polymer + Ar plasma are −0.767 eV, −0.826 eV, −0.771 eV and −0.827 eV. These values for $(E_{ox})_{on}$ and $(E_{red})_{on}$ are correlated linearly with HOMO and LUMO energy with a correction factor of 4.4 eV. The HOMO and LUMO values deduced from CV measurements for the polymer and treated polymer are reported in Table 1. The HOMO energy levels of control polymer and polymer + N_2 plasma were found to be between −4.763 and −4.878 eV, whereas the LUMO energy levels of control polymer and polymer + N_2 plasma were found to be between −3.633 and −3.629 eV with a small variation, which shows that both HOMO and LUMO levels were modified to an appreciable extent using APPJ. Apparently, the more powerful the acceptor, the higher the electron affinity, which finally leads to lower-lying LUMO level in these polymers, although on treating the polymer with plasma, we can modify its bandgap and increase its utility to a larger extent. To further

investigate the surface properties of the polymer, we continued with conductivity measurements and AFM.

3.3 Conductivity and surface roughness measurements of polymer and modified polymer

Nowadays, the improvement in the conductivity of polymers is a very important issue. There are numerous ways to enhance the conductivity of polymers by adding secondary dopants or additives such as several alcohols and high-boiling-point solvents.[35,36] Still, these methodologies suffer from many limitations, so we tried to enhance the conductivity by utilizing a plasma in the work reported here. Our experimental conductivity results displayed in Table 2 show that the conductivity of the polymer is 7.0×10^{-5} S cm^{-1} at 25 °C, whereas after plasma treatment, the conductivity of the polymer increased. After treating the polymer with plasma operating with air, Ar and N_2 gases, the conductivity of the polymer was found to be 3.1×10^{-4}, 3.3×10^{-3} and 6.3×10^{-3} S cm^{-1}, respectively. The N_2 plasma-treated polymer had maximum conductivity, whereas the air plasma-treated polymer had minimum conductivity. In any case, the plasma-treated polymer irrespective of feeding gases had a greater conductivity than the control polymer. Therefore, we concluded that the conductivity of polymer increased to a greater extent on plasma treatment.

To gain insight into the conductivity enhancement of the polymer after treatment with APPJ operating with different feeding gases, we investigated the surface morphology of control polymer and plasma-modified polymer using AFM. The modification of PHVTT polymer with plasma treatment resulted in a decrease of average surface roughness. The surface morphology of polymer and plasma-modified polymer is shown in Fig. 3. It is obvious that PHVTT (control polymer) exhibits more surface roughness in comparison to the modified polymer surface. During plasma treatment, ablation of the polymer surface takes place with a different ablation rate of amorphous and crystalline phases that resulted in the appearance of the amorphous structures on the plasma-modified polymer surface. The control polymer showed an average roughness (R_a) of about 38.048 nm, while after air plasma treatment $R_a = 9.830$ nm. This reveals that the plasma treatment of the polymer surface makes it smoother. After the Ar plasma treatment, R_a of the polymer comes out to be 9.236 nm, again suggesting that Ar plasma treatment makes the polymer surface smoother than air plasma treatment, whereas $R_a = 8.820$ nm for the N_2 plasma-treated polymer reveals that this treatment has greater tendency to smoothen and minimize the roughness of the polymer as compared to plasma operating with other feeding gases. This could be the important factor for

Table 2 Conductivity of polymer and polymer treated with plasma in different feeding gases

Sample	Conductivity (±0.4 S cm^{-1})
Polymer	7.0×10^{-5}
Polymer + air	3.0×10^{-4}
Polymer + N_2	6.0×10^{-3}
Polymer + Ar	3.0×10^{-3}
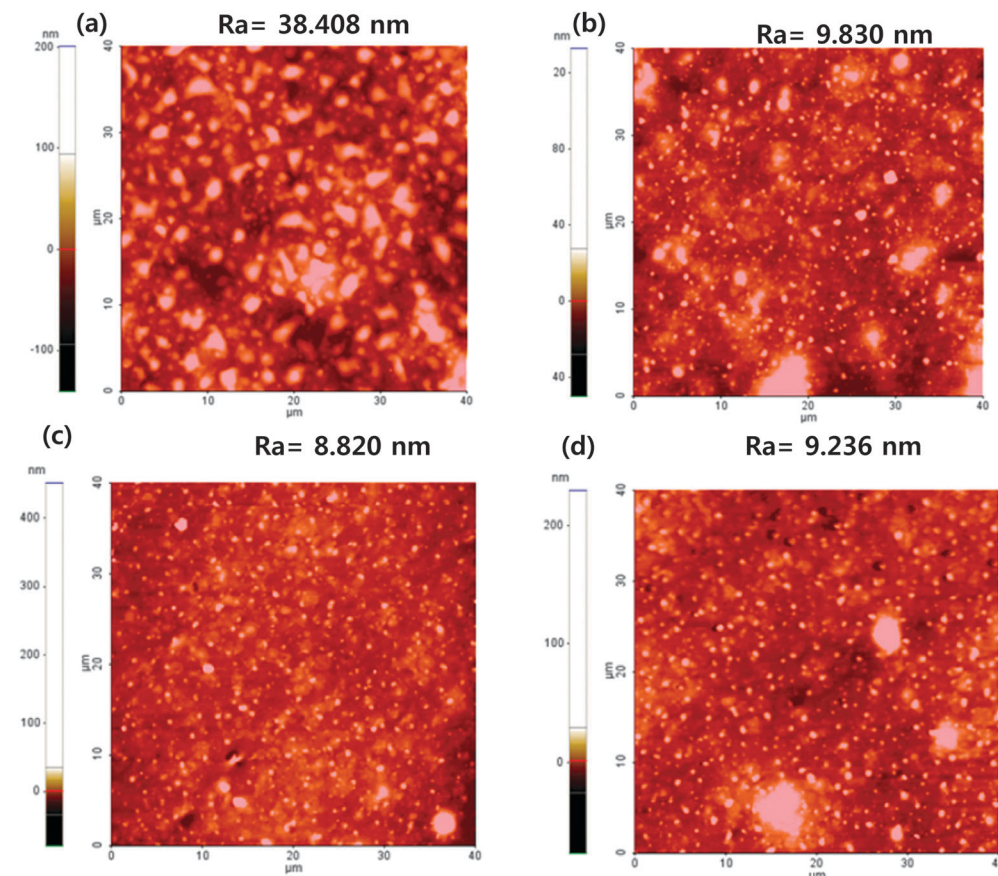
Fig. 3 AFM images of thin films cast from (a) polymer, (b) polymer treated with air plasma, (c) polymer treated with N_2 plasma and (d) polymer treated with Ar plasma. The scan size for all images is 40 mm × 40 mm.

enhancing the conductivity of the polymer after the N_2 plasma treatment.

3.4 Characterization of polymer and modified polymer surface using X-ray photoelectron spectroscopy

The influence of plasma treatment on the polymer surface was studied using XPS. The PHVTT samples modified by APPJ plasma operating with the different feeding gases were analyzed. The results from XPS measurements are summarized in Fig. S5 to S8 (ESI†). The chemical structure of PHVTT consists of carbon, sulfur and nitrogen in the basic polymer chain, while after plasma treatment, we observed the generation of oxygen that results in the structural changes or oxidation of the polymer. The control polymer has no oxygen in its structure; therefore, the changes in oxygen concentration after plasma treatment can be traced successfully. Further, all peaks of control polymer and modified polymer were examined using the previous literature, and are provided in Fig. S5 to S8 (ESI†).[37–44]

The C 1s core level spectrum of the control polymer is illustrated as Fig. S5 (ESI†). The binding energies were corrected by taking the C 1s core level at 284.6 eV for all samples.[45,46] The peaks at 284.2, 285.7, 286.7, and 290.1 eV correspond to C–C, C–S, C=N groups of the polymer and the $\pi \rightarrow \pi^{\star}$ shake up signals from the thiophene ring, respectively. The C 1s spectrum of the modified polymer after air plasma treatment revealed peaks at 284.2, 286.2 and 287.6 eV corresponding to C–C, C=N and C=O groups, respectively. Thus, the addition of oxygen in the air plasma as compared to the control polymer resulted in the modification of the polymer surface, whereas in the case of Ar plasma-treated polymer, we detected peaks at 284.2, 285.9 and 287.2 eV corresponding to C–C, C–O and C=O groups, respectively, the C=N being replaced with C–O group after the Ar gas plasma treatment. On the other hand, after N_2 plasma treatment of the polymer, we observed peaks at 284.2 and 285.9 eV that correspond to C–C and C–O of the modified polymer, respectively. Here, the peak appearing at 287 eV in the case of all other plasma treatments is absent and thus it suggests that the N_2 plasma modifies the polymer to a greater extent.

Similarly, O 1s core level spectra are illustrated in Fig. S6 (ESI†) which shows that O 1s is absent, because of the absence of oxygen moiety in the polymer, whereas the oxygen peak appeared in the spectra of the plasma-treated polymer samples. The O 1s spectrum of the air plasma-modified polymer revealed peaks at 531.0, 532.1, 532.8 and 534.1 eV corresponding to O=C–N, O=C–O, C–O–C or C–O–H, and O=C–O–C groups, respectively, whereas after Ar plasma treatment, we observed peaks for modified polymer at 531.1, 532.2 and 534.1 eV corresponding to O=C–N, O=C–O, and O=C–O–C groups, respectively. The peaks corresponding to C–O–C or C–O–H groups were absent in this case as compared with air plasma-treated polymer.

Further, in the case of N_2 plasma-treated polymer, we observed peaks at 531.2 and 532.9 eV which again corresponded to O=C–N and C–O–C or C–O–H groups, respectively. The peaks at 532.1 and 534.1 eV were present in the case of other feeding gas plasma source treatment of the polymer, but these were found to be absent in the case of the N_2 plasma-treated polymer. This again suggests that the N_2 plasma modified the polymer to a greater extent and selectivity of the polymer increases by changing the feeding gases in APPJ.

The N 1s core level spectrum is illustrated as Fig. S7 (ESI†). The N 1s core level spectrum of the control polymer showed a peak at 399.9 eV corresponding to C=N group of the polymer. The N 1s spectrum of the polymer modified with air plasma treatment revealed peaks at 398.0, 402.1 and 405.2 eV, corresponding to C=N, NH_2^+ and NO or NO_2 groups of the polymer. Thus, the presence of oxygen in the polymer after the air plasma treatment as compared to the control polymer is due to the modification of the polymer surface by the plasma treatment, while for Ar plasma-treated polymer, we observed peaks at 397.1, 403.1 and 407.6 eV corresponding to C=N, NH_2^+ and NO or NO_2 groups, respectively. Hence the results are similar to those for the air plasma-treated polymer, with a difference of more intense peaks in the case of the Ar plasma-treated polymer, whereas for the N_2 plasma-treated polymer, we observed peaks at 397.9, 402.9 and 405.2 eV corresponding to C=N, NH_2^+ and NO groups, respectively. The peaks in all cases of the APPJ feeding gases are the same but the intensity of the peaks is less in the case of the N_2 plasma-treated polymer as compared to the other plasma sources.

Typical S 2p spectra of the polymer before and after the plasma treatment are shown in Fig. S8 (ESI†). The spectra showed two S 2p bands, each corresponding to a doublet of S $2p_{3/2}$ and S $2p_{1/2}$ components with spin–orbit splitting and having a 2 : 1 intensity ratio. The weaker S $2p_{3/2}$ peak at 163.9 eV and the stronger S $2p_{3/2}$ peak at 167.1 eV correspond to sulfur atoms of the polymer, respectively. The S 2p spectrum of the air plasma-modified polymer revealed peaks at 161.1, 163.0, 163.9, 166.2 and 169.3 eV corresponding to absorption by lone "S", C–S–C, S–H, and S-atom and oxidized sulfur of the polymer. Thus, the presence of oxygen in the air plasma resulted in the modification of the polymer surface, while the Ar plasma-treated polymer showed peaks at 162.9, 163.8 and 166.2 eV corresponding to C–S–C, S–H groups and S-atom respectively, with an absence of the oxidized sulfur peak. This also reveals that more oxidation of the polymer occurs in the presence of air plasma than Ar plasma, whereas for the N_2 plasma-treated polymer, we detected peaks at 163.1, 164.0 and 166.3 eV corresponding to C–S–C, S–H groups, and S-atom respectively. Hence, use of Ar and N_2 plasmas resulted in controlled modification of the polymer, whereas use of air plasma resulted in modification of the polymer to a greater extent, with the formation of oxidized sulfur. Hence, we can also predict the surface modification of the low bandgap polymer using XPS. In order to examine the bulk modification of the polymer, we have further measured the work function using γ-FIB and CL.

3.5 Characterization of bulk modification of polymer using γ-FIB and CL

The measurement of the work function of a polymer before and after APPJ treatment with different feeding gases is an important factor for determining the mechanism of the increase in conductivity of the polymer after plasma treatment.[27] The work function was calculated using the γ-FIB system; the results are shown in Fig. 4a and Table 3. The work function of the control polymer was calculated to be 11.11 eV, whereas after the air plasma treatment the work function of the polymer was measured as 9.88 eV. Additionally, the work function of the polymer after the Ar and N_2 plasma treatments was found to be 9.86 and
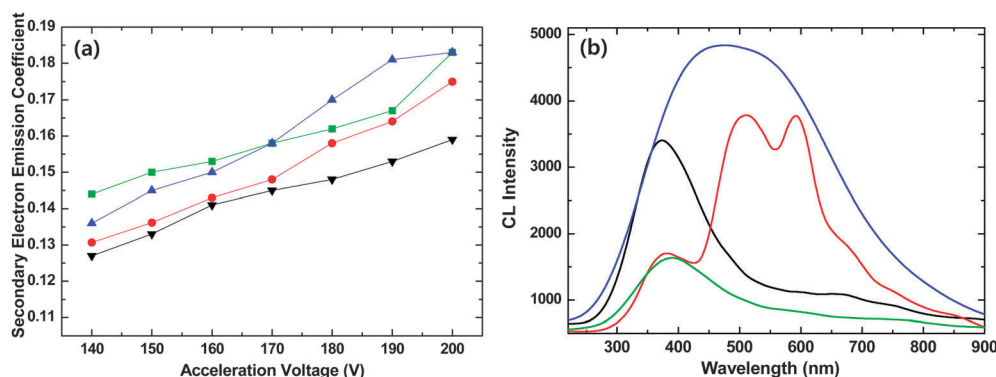
Fig. 4 (a) Secondary electron emission coefficient and (b) cathodoluminescence (CL) spectrum intensity of polymer (black), polymer treated with air plasma (red), polymer treated with N_2 plasma (blue) and polymer treated with Ar plasma (green).

Table 3 Work function of polymer and polymer treated with plasma with different feeding gases

	Control	Air	N_2	Ar
Work function (eV)	11.11 (±0.006)	9.88 (±0.007)	9.56 (±0.004)	9.86 (±0.005)

9.56 eV, respectively. Therefore, we found that after the plasma treatment the work function decreases very fast as compared to that of the control polymer.

Subsequently, we studied the CL[27] of the polymer both before and after the plasma treatment, as displayed in Fig. 4b. Here, similar results were obtained and were correlated with the above experimental data as maximum red shift and an increase in the intensity was observed for the N_2 plasma-treated polymer. After air plasma treatment of the polymer, the red shift was seen with the appearance of an additional peak which suggests that there is formation of some sub-levels in the structure of the polymer after the air plasma treatment. Additionally, a reduction with a slight red shift was observed in the case of the Ar plasma-treated polymer. The observed difference in the spectra of control polymer and polymer after plasma treatment with different feeding gases could be due to the change in the crystal polymorphs of the polymer. Hence, CL data also support our results discussed above and suggest that there is a considerable change in the low bandgap polymer after plasma treatment, which in turn modifies its physical and optical properties to a greater extent.

3.6 Increase in power conversion efficiency of bulk heterojunction solar cells

Bulk heterojunction solar cells were fabricated with a sandwich structure of ITO/PEDOT:PSS/PHVTT:$PC_{71}BM$/LiF/Al. After deposition of the PEDOT:PSS layer on the top of the anode (ITO), the active materials were deposited via spin coating from 1,2-dichlorobenzene solution of PHVTT polymer and $PC_{71}BM$. The resulting films were dried under vacuum at room temperature for 4 h, and then annealed at 90 °C for 10 min to remove the solvent. For the bulk heterojunction solar cells, the $PC_{71}BM$ was used as an electron acceptor and polymers were used as electron donor. The J–V characteristics of the polymer solar cells prepared from the treated and untreated polymer:$PC_{71}BM$ blend materials are shown in Fig. 5. The short circuit current density (J_{SC}),

open circuit voltage (V_{OC}), fill factor (FF), power conversion efficiency (PCE), series resistances (R_{SR}) and shunt resistance (R_{SH}) of these devices are summarized in Table 1 and Fig. 5. For these devices based on the PHVTT (with or without plasma treatment):$PC_{71}BM$ blend materials, an improvement in performance was observed for treated polymer as compared to control polymer. The PCEs of the control polymer and air, Ar and N_2 plasma-treated polymer devices were found to be 4.11%, 4.83%, 4.87% and 5.14%, respectively. Although the polymer exhibited a low optical bandgap and broadest absorption spectrum, the low LUMO level hindered the efficient exciton dissociation, resulting in a low PCE of 4.11%. These results are similar to those of Chen et al., where at lowest optical bandgap low PCE was observed and high PCE was observed at high bandgap.[47] The polymer modified with the nitrogen plasma showed more red-shift, a broader absorption spectrum, high mobility, high bandgap and a higher PCE of 5.14%. In view of this fact, the polymer modified with the nitrogen plasma showed a higher bandgap with intense absorption in the visible region. Although the air plasma- and Ar plasma-treated polymers also showed a red-shift, a broader absorption spectrum, high mobility, and a higher PCE of 4.83 and 4.87% respectively, these were less as compared to the N_2 plasma-treated polymer. One of the reasons is that higher V_{oc} is obtained for the N_2 plasma-treated polymer as compared to the other treated polymers. It is reported by Chen et al.[48] that V_{oc} in a low bandgap polymer is one of the critical factors towards higher PCE. Hence, plasma treatment not only changes the surface properties, but also modifies the bandgap between HOMO and LUMO (bulk properties) and also increases the PCE (as shown in Scheme 1 and Table 1).

To gain insight into the action of APPJ operating with different feeding gases on solid phase polymer, we further concentrated on the emission spectra as illustrated in Fig. 1, Fig. S1 and S2 (ESI†). The spectra clearly elucidate the molecular NO β, γ system, superoxide anion O_2^*, OH molecules and N_2(C–B) second positive system to be prominent for the N_2 plasma-treated polymer, as compared to the case of Ar plasma- and air
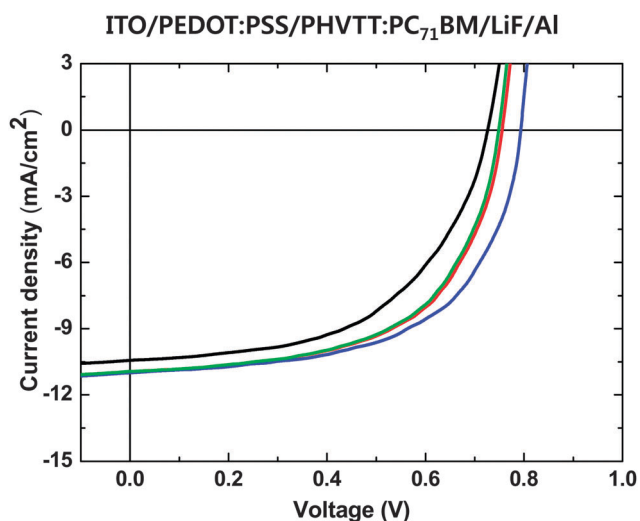
Fig. 5 J–V characteristics of PSCs fabricated using polymer (black), polymer treated with air plasma (red), polymer treated with N_2 plasma (blue) and polymer treated with Ar plasma (green).
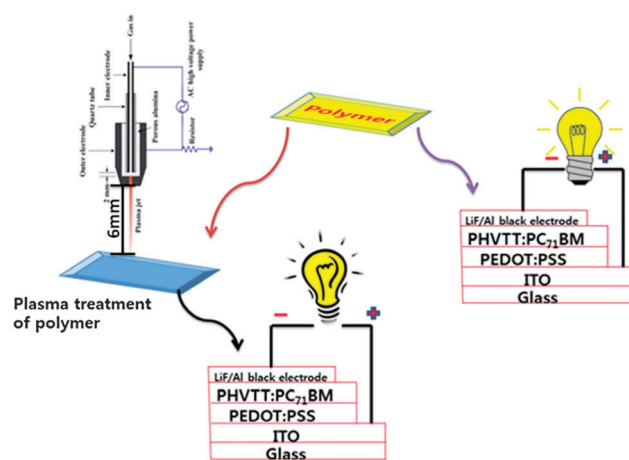
Scheme 1 Schematic diagram for the increase in power conversion efficiency (PCE) of the bulk heterojunction photovoltaic cells in the presence of the plasma-modified polymer.

27050 | Phys. Chem. Chem. Phys., 2014, 16, 27043–27052

This journal is © the Owner Societies 2014

plasma-treated polymers. And, N_2^+(B–X) and N_2(B–A) lines were found to be absent in the case of all plasmas except the air plasma. Moreover, intense emission lines from the O_2 first negative system were observed for the air plasma- and Ar plasma-treated polymers, as compared to the N_2 plasma-treated polymer. These different levels of radicals originating from the different feeding gases lead to different levels of modification. Plasma provides a reactive environment for the polymer surface. We observed that physical–chemical reaction occurred after plasma treatment that resulted in breaking of some chemical bonds, creation of some active sites near polar groups, modification of functional groups, *etc.* During this interaction of reactive species generated by plasma on polymer surfaces, reactions such as functionalization and intermolecular cross-linking occurred. Some of the reactions might be as follows:

$$R - H \rightarrow R^0 + H^0$$

$$R^0 + O_2 \rightarrow ROO^0$$

$$O_2 \rightarrow O^0 + O^0$$

$$R^0 + O^0 \rightarrow R^0 + ROOH$$

$$R^0 + O^0 \rightarrow ROOR$$

$$ROOH \rightarrow RO^0 + OH^0$$

$$RO^0 + H^0 \rightarrow ROH$$

$$RO^0 + OH^0 \rightarrow ROOH$$
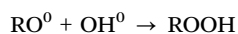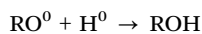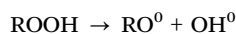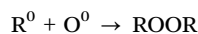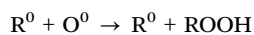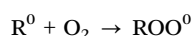
where R is an alkyl group. Many more reactions are possible that can modify the polymer. However, the VUV photons can generate various oxidation products such as –C–OH, –C=O, –C–O–C, –COOH groups *etc.*[49] Therefore, these are the main cause for the change in XPS peaks in the case of different feeding gas plasmas, resulting in the different extent of modification of the functional groups. Moreover, the changes in AFM topography measurements showed the smoothening of the polymer surface after the plasma treatment. This could possibly be due to the cross-linking of polymer bonds (mainly in amorphous phase) resulting in high mobility of radicals. These radicals are readily oxidized and preferential etching takes place in the amorphous region.[49] This might again be the cause of changes in CL spectra after the plasma treatment of polymer. The plasma jet with air feeding gas showed a greater red shift in the CL spectra, as compared with the other feeding gases, due to the generation of more radicals in air plasma resulting in extensive cross-linking of the polymer. And this results in lower PCE of solar cell as compared with the polymer treated with the other feeding gas plasmas.

4. Conclusion

Our experimental data show that the structure of a polymer can be modified using plasma with different feeding gases. UV-visible spectroscopy results reveal that a red shift is observed for all plasma-treated polymers, which helps in harvesting more sunlight of longer wavelength. PL, CV, Raman spectroscopy and XPS experimental data indicated that physical and chemical properties of the polymer changed drastically after the plasma treatment. We also observed that the conductivity of the polymer increased after the plasma treatment with a decrease in roughness of the film after treatment. Likewise, PCE also increased after the treatment of the polymer with plasma. All these results led us to conclude that the maximum physical and chemical changes occurred in the N_2 plasma-treated polymer due to presence of limited types of radicals, while the presence of more than one type of radicals in the air plasma increases the probability of converting reactive radical species to stable species. To summarize, all these radicals modify the polymer surface to different extents without destroying the polymer.

Acknowledgements

References

1 E. D. Kirson, V. Dbaly, F. Tovarys, J. Vymazal, J. F. Soustiel, A. Itzhaki, D. Mordechovich, S. Steinberg-Shapira, Z. Gurvich, R. Schneiderman, Y. Wasserman, M. Salzberg, B. Ryffel, D. Goldsher, E. Dekel and Y. Palti, *Proc. Natl. Acad. Sci. U. S. A.*, 2007, **104**, 10152–10157.

2 E. A. Ratovitski, X. Cheng, D. Yan, J. H. Sherman, J. Canady, B. Trink and M. Keidar, *Plasma Process. Polym.*, 2014, DOI: 10.1002/ppap.201400071.

3 D. Staack, A. Fridman, A. Gutsol, Y. Gogotsi and G. Friedman, *Angew. Chem., Int. Ed.*, 2008, **47**, 8020–8024.

4 S. Ptasinska, B. Bahnev, A. Stypczynska, M. Bowden, N. J. Mason and N. S. Braithwaite, *Phys. Chem. Chem. Phys.*, 2010, **28**, 7779–7781.

5 G. Li, H.-P. Li, L.-Y. Wang, S. Wang, H.-X. Zhao, W.-T. Sun, X.-H. Xing and C.-Y. Bao, *Appl. Phys. Lett.*, 2008, **92**, 221504.

6 P. Attri, P. Venkatesu, N. Kaushik and E. H. Choi, *RSC Adv.*, 2012, **2**, 7146–7155.

7 P. Attri and E. H. Choi, *PLoS One*, 2013, **8**, e75096.

8 P. Attri, J. H. Park, J. Gaur, N. Kumar, D. H. Park, S. N. Jeon, B. S. Park, S. Chand, H. S. Uhm and E. H. Choi, *Phys. Chem. Chem. Phys.*, 2014, **16**, 18375–18382.

9 J. Julak, O. Janouskova, V. Scholtz and K. Holada, *Plasma Processes Polym.*, 2011, **8**, 316–323.

10 G. Bruno, P. Capezzuto and A. Madan, *Plasma Deposition of Amorphous Silicon-Based Materials*, Academic Press, San Diego, 1995.

11 R. Wilhelm, Deposition properties and applications of carbon-based coatings, in *Advanced Technologies Based on Wave and Beam Generated Plasmas*, ed. H. Schluter and A. Shivarova, NATO Sci. Series, Kluwer, Dordrecht, 1999, vol. 67, pp. 123–135.

12 H. K. Yasuda, *Plasma Polymerization and Plasma Interactions with Polymeric Materials*, Wiley, New York, 1990.

13 Z. Ding, J. Chen, Sh. Gao, J. Chang, J. Zhang and E. T. Kang, *Biomaterials*, 2004, **25**, 1059–1067.

14 K. Kim, C. Kim and Y. Byun, *Biomaterials*, 2004, **25**, 33–41.

15 O. Goossens, E. Dekempeneer, D. Vangeneugden, R. Van de Leest and C. Leys, *Surf. Coat. Technol.*, 2001, **142–144**, 142–144.

16 J.-H. Kim, C. E. Song, I.-N. Kang, W. S. Shin and D.-H. Hwang, *Chem. Commun.*, 2013, **49**, 3248–3250.

17 L. Dou, J. You, J. Yang, C.-C. Chen, Y. He, S. Murase, T. Moriarty, K. Emery, G. Li and Y. Yang, *Nat. Photonics*, 2012, **6**, 180–185.

18 R. Tautz, E. D. Como, T. Limmer, J. Feldmann, H.-J. Egelhaaf, E. von Hauff, V. Lemaur, D. Beljonne, S. Yilmaz, I. Dumsch, S. Allard and U. Scherf, *Nat. Commun.*, 2013, **3**, 1–8, DOI: 10.1038/ncomms1967.

19 P. T. Boudreault, A. Najari and M. Leclerc, *Chem. Mater.*, 2011, **23**, 456–469.

20 J. Hou, H.-Y. Chen, S. Zhang, G. Li and Y. Yang, *J. Am. Chem. Soc.*, 2008, **130**, 16144–16145.

21 Y. Liang, D. Feng, Y. Wu, S.-T. Tsai, G. Li, C. Ray and L. Yu, *J. Am. Chem. Soc.*, 2009, **131**, 7792–7799.

22 V. Gupta, N. Chaudhary, R. Srivastava, G. D. Sharma, R. Bhardwaj and S. Chand, *J. Am. Chem. Soc.*, 2011, **133**, 9960–9963.

23 C. Piliego, T. W. Holcombe, J. D. Douglas, C. H. Woo, P. M. Beaujuge and J. M. J. Frechet, *J. Am. Chem. Soc.*, 2010, **132**, 7595–7597.

24 B. Walker, A. B. Tamayo, X.-D. Dang, P. Zalar, J. Hwa Seo, A. Garcia, M. Tantiwiwat and T.-Q. Nguyen, *Adv. Funct. Mater.*, 2009, **19**, 3063–3069.

25 G. Yu, J. Gao, J. C. Hummelen, F. Wudl and A. J. Heeger, *Science*, 1995, **270**, 1789–1791.

26 P. Attri, S. H. Lee, S. W. Hwang, J. I. Kim, S. W. Lee, G. C. Kwon, E. H. Choi and I. T. Kim, *PLoS One*, 2013, **88**, e68970.

27 J. H. Choi, C. G. Son, Y. J. Hong, B. C. Park, H. S. Uhm and E. H. Choi, *Adv. Nat. Sci.: Nanosci. Nanotechnol.*, 2010, **1**, 045014.

28 D. H. Apaydın, D. E. Yıldız, A. Cirpana and L. Toppare, *Sol. Energy Mater. Sol. Cells*, 2013, **113**, 100–105.

29 L. Beverina and G. A. Pagani, *Acc. Chem. Res.*, 2014, **47**, 319–327.

30 J. W. Chen and Y. Cao, *Acc. Chem. Res.*, 2009, **42**, 1709–1718.

31 M. He, M. Wang, C. Lin and Z. Lin, *Nanoscale*, 2014, **6**, 3984–3994.

32 P. Slepicka, S. Trostova, N. S. Kasalkova, Z. Kolska, P. Sajdl and V. Svorcık, *Plasma Processes Polym.*, 2012, **9**, 197–206.

33 J. B. Pawley, *Handbook of Biological Confocal Microscopy*, Kluwer Academic Publishers, Dordrecht, 1995.

34 M. Schmitt, B. Leimeister, L. Baia, B. Weh, I. Zimmermann, W. Kiefer and J. Popp, *ChemPhysChem*, 2003, **4**, 296–299.

35 J. Ouyang, Q. F. Xu, C. W. Chu, Y. Yang, G. Li and J. Shinar, *Polymer*, 2004, **45**, 8443–8450.

36 B. Y. Ouyang, C. W. Chi, F. C. Chen, Q. Xu and Y. Yang, *Adv. Funct. Mater.*, 2005, **15**, 203–208.

37 G. P. Lopez, D. G. Castner and B. D. Ratner, *Surf. Interface Anal.*, 1991, **17**, 267–272.

38 R. Memarzadeh, F. Panahi, S. Javadpour, A. Khalafi-Nezhad, H.-B. Noh and Y.-B. Shim, *Bull. Korean Chem. Soc.*, 2012, **33**, 1297–1302.

39 W. Zhang, S. Lin, C. Wang, J. Hu, C. Li, Z. Zhuang, Y. Zhou, R. A. Mathies and C. J. Yang, *Lab Chip*, 2009, **9**, 3088–3094.

40 K. Strzelec, N. Baczek, M. Szynkowska and J. Grams, *J. Appl. Polym. Sci.*, 2014, **131**, 40330–40339.

41 H. Hwang, H. Kim, S. Nam, D. D. C. Bradley, C. S. Ha and Y. Kim, *Nanoscale*, 2011, **3**, 2275–2279.

42 R. H. Sestrem, D. C. Ferreira, R. Landers, M. L. A. Temperini and G. M. do Nascimento, *Eur. Polym. J.*, 2010, **46**, 484–493.

43 P. Pfluger, M. Krounbi, G. B. Street and G. Weiser, *J. Chem. Phys.*, 1983, **78**, 3212–3218.

44 F. Wang, H. Luo, Q. Wang, J. Wang and J. Xu, *Molecules*, 2009, **14**, 4737–4746.

45 R. Li, X. Tao and X. Li, *J. Mater. Chem.*, 2009, **19**, 983–987.

46 R. Li, L. Bao and X. Li, *CrystEngComm*, 2011, **13**, 5858–5862.

47 C. H. Chen, C. H. Hsieh, M. Dubosc, Y. J. Cheng and C. S. Hsu, *Macromolecules*, 2010, **43**, 697–708.

48 H.-Y. Chen, J. Hou, S. Zhang, Y. Liang, G. Yang, Y. Yang, L. Yu, Y. Wu and G. Li, *Nat. Photonics*, 2009, **3**, 649–653.

49 A. C. Fozza, J. E. Klemberg-Sapieha and M. R. Wertheimer, *Plasmas Polym.*, 1999, **4**, 183–206.